FIRST PRINCIPLE STUDY OF BALLISTIC THERMAL CONDUCTANCE OF GRAPHENE ANTIDOT LATTICES FOR THERMOELECTRIC APPLICATIONS

H. Karamitaheri [1*], M. Pourfath [1], N. Neophytou [1], M. Pazoki [2], and H. Kosina [1]

[1] *Institute for Microelectronics, TU Wien, Vienna, Austria*
[2] *Department of Physics, Sharif University of Technology, Tehran, Iran*
[*] E-mail: karami@iue.tuwien.ac.at

ABSTRACT

In this work we present a first-principles study of lattice thermal properties of edge-hydrogen-passivated graphene antidot lattices of different dot shapes. We calculate the phononic bandstructure of antidot lattices with hexagonal, triangular and rectangular shapes. Using the Landauer transport formalism and ballistic transport considerations, we calculate the lattice thermal conductance. We show that in graphene antidot lattices with 80% fill-factor, the thermal conductance could be drastically reduced to 15%-20% of the pristine graphene value, depending on the shape of the dot. The reduction is larger for the triangular antidots because for the same fill factor, they have the longest boundary and the smallest distance between neighboring antidots. Our results could provide guidance in the design of graphene based thermal and thermoelectric devices.

1. INTRODUCTION

Thermoelectric devices convert heat into electricity and vise versa. The efficiency of thermoelectric devices depends on the ZT figure of merit defined as:

$$ZT = \frac{S^2 GT}{K_{el} + K_{ph}} \quad (1)$$

where S denotes the Seebeck coefficient, G is the electrical conductance, T is the temperature, K_{el} and K_{ph} are the electrical and the lattice parts of the thermal conductance, respectively [1]. A good thermoelectric material, therefore, should simultaneously have a high Seebeck coefficient, a high electrical conductance, and a low thermal conductance. The interdependence of these parameters, however, has kept ZT low. Some of the best thermoelectric materials such as Bi_2Te_3 exhibit $ZT \sim 1$ [2], but suffer from high cost, and material abundance. Other common and inexpensive materials such as bulk silicon have a very low $ZT \approx 0.01$ [3] because of high thermal conductivity. Recently, nanostructured thermoelectric materials have been given significant attention because of the possibility of independently controlling the parameters that determine ZT and, thus, achieving high thermoelectric performance [4-6]. A large reduction in the lattice part of the thermal conductivity has been reported for nanostructures based on Si, Bi_2Te_3, Pb_2Te_3, SiGe superlattices and other materials [6-8], that resulted in significant improvements in the ZT figure of merit.

Graphene, a recently discovered form of carbon, has received significant attention over the last few years due to its excellent electrical, optical, and thermal properties [9-11]. A method to produce graphene sheets at large scale has also been reported [12]. Specifically for thermoelectrics, although the electrical conductivity of graphene is as high as that of copper [13], due to its zero bandgap it has a low Seebeck coefficient [14] and therefore a low power factor. On the other hand, several schemes for achieving a bandgap have been demonstrated [15,16], which places graphene as a potential candidate for thermoelectric applications. For this, however, its high thermal conductivity (an order of magnitude higher than that of copper [17]), needs to be significantly reduced. The high thermal conductance of graphene is mostly due to the lattice contribution, whereas the electrical contribution to the thermal conductance is minimal [17,18]. Therefore, one can design its total thermal conductance by focusing on phonon transport engineering.

Recently many theoretical studies have been performed on the thermal conductivity of graphene and graphene-based structures such as graphene nanoribbons (GNRs). It has been shown that boundaries, edge roughness, and even strain can strongly reduce the thermal conductance [19,20]. Vacancies, defects, and isotope doping could also have a strong influence [21,22].

In this work, we examine the lattice thermal properties of graphene antidot lattices with ~80% fill factor using first-principle calculations and ballistic transport considerations. We examine different shapes of antidots. Consistent with the previous works regarding different type of graphene lattice modifications, we find that the lattice thermal conductivity is significantly reduced with the introduction of antidots in the pristine lattice.

2. APPROACH

Graphene antidot lattices (GAL) are geometrical structures as shown in Fig. 1, where antidots are formed periodically in the graphene lattice [23]. The antidots can have different shapes and sizes and, thus, the antidot lattices different fill factors. Such structures, with antidot

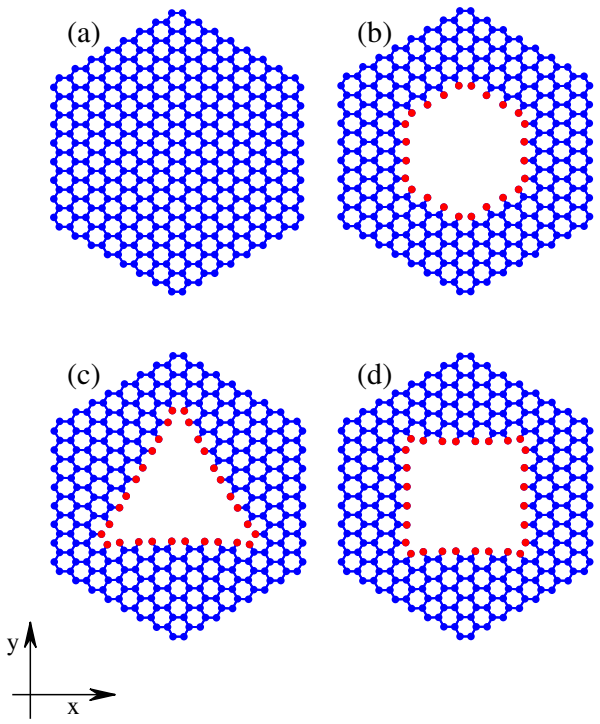

Fig. 1: Geometrical structures of different GALs. (a) Pristine graphene. (b) Hex(8,96,24). (c) IsoTri (8,90,30). (d) Rect(8,104,24). Hydrogen atoms are shown in red color. Transport assumed to be along the x-direction.

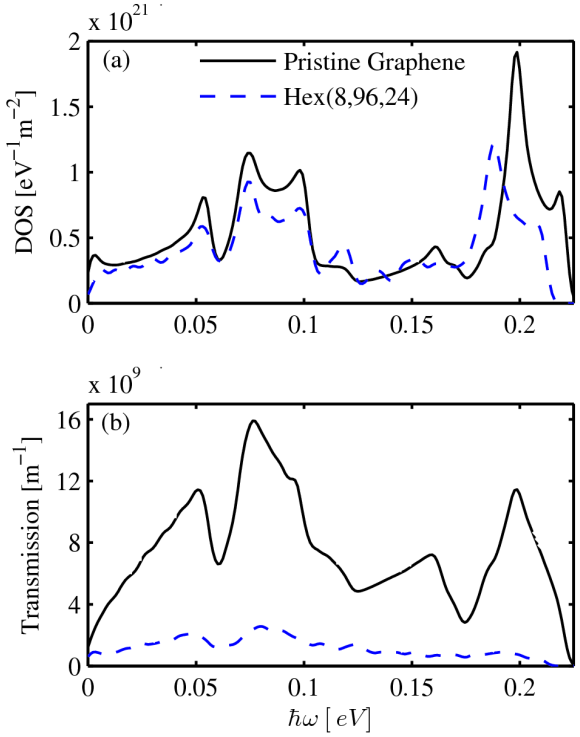

Fig. 2: Comparison between (a) density of states and (b) transmission of pristine graphene and Hex(8,96,24).

spacing below 100 nm have been recently experimentally realized [24], and have been proposed for electrical and optical applications [16,23]. Theoretical studies, also indicate that by introducing regular array of antidots in the semi-metallic graphene sheet, it is possible to achieve a direct bandgap [16]. In this paper we investigate the lattice thermal properties of GALs using first-principle calculations. The unit cell of a hydrogen-passivated GAL can be described by three parameters (L, N_C, N_H), where L is the side length of the hexagon in the units of the graphene lattice constant (a=2.46Å), N_C is the number of carbon atoms removed from the pristine supercell, and N_H is the number of hydrogen atoms that passivate the edge carbon atoms. In Fig. 1 Hex, IsoTri, and Rect represent a hexagonal, iso-triangular, and rectangular antidot in the hexagonal unit cell, respectively. We passivate all the dangling bonds at the edges of the antidots with hydrogen atoms using a carbon-hydrogen bond of 1.1Å length [25].

To study the phononic bandstructure of hydrogen-passivated GALs the ab-initio simulation package SIESTA is employed [26]. We use a double zeta polarized basis set with a mesh cut-off 125 Ry. The general gradient approximation is used for the exchange correlation potential with a functional proposed by Perdew et al. [27]. Brillouin zone sampling was carried out by a 10×10×1 Monkhorst-Pack grid. For structural relaxation, the positions of the atoms are changed until the force acting on each atom becomes smaller than 0.03-eV/Å. Self consistency in the total energy is achieved with a tolerance of less than 10^{-4} Ry. For phonon calculations, the force constant matrix is calculated by displacing each atom 0.04 Bohr along the coordinate directions around its equilibrium position and evaluating the forces exerted by the other atoms.

Using the phononic bandstructures, the density of modes is calculated, and from this the ballistic transmission $T_{ph}(E)$ is extracted. In the ballistic limit the transmission can be extracted from the density of modes $M_{ph}(E)$ [28]:

$$T_{ph}(E)|_{Ballistic} = M_{ph}(E) = \sum \delta\left(E - \varepsilon_{ph}(k)\right) \Delta k_{\perp} \frac{\partial \varepsilon_{ph}(k)}{\partial k_{\parallel}} \qquad (2)$$

where δ is the delta function, $k_{\perp}$ refers to the wave vector component perpendicular to the transport direction and $k_{\parallel}$ to the wave vector component parallel to the transport direction. Once the transmission is obtained, the transport coefficient is calculated within the framework of the ballistic Landauer theory as:

$$K_{ph} = \frac{1}{h} \int T_{ph}(\omega) \hbar\omega \frac{\partial n(\omega)}{\partial T} d(\hbar\omega) \qquad (3)$$

Where $n(\omega)$ denotes the Bose-Einstein distribution function [29].

3. RESULTS AND DISCUSSION

Figure 2 compares the phonon density of states (DOS) and the transmission of the the pristine graphene (solid-

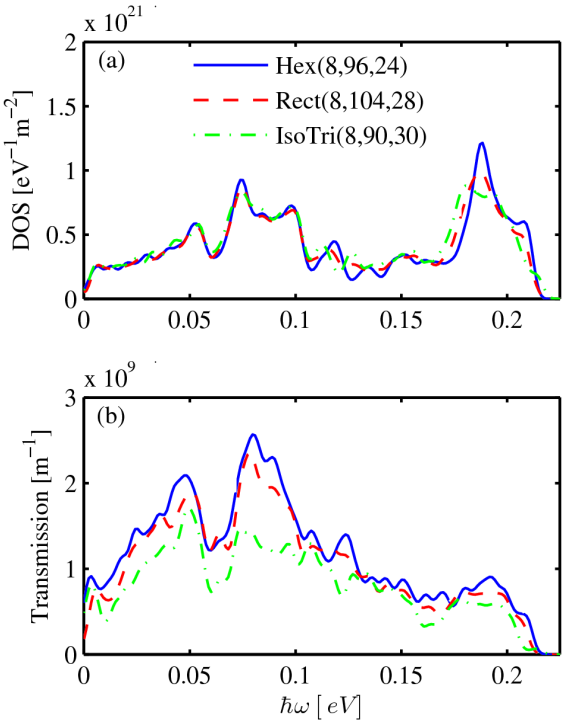

Fig. 3: Comparison between (a) phonon density of states and (b) transmission of different GALs.

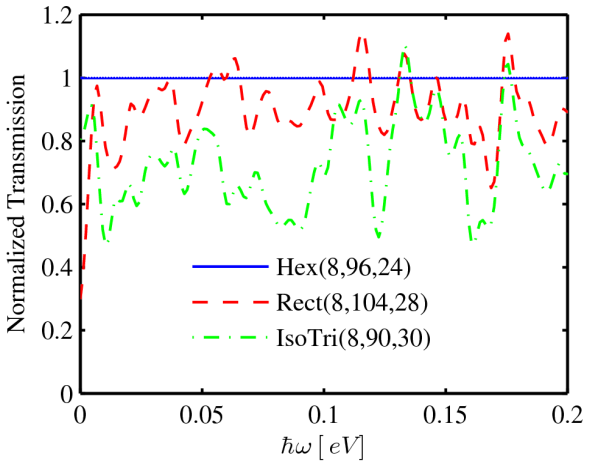

Fig. 4: Transmission of the IsoTri(8,90,30) and Rect(8,104,28) GALs normalized to the transmission of the Hex(8,96,24).

black line) to those of the Hex(8,96,24) GAL (dashed-blue line). The GAL DOS in Fig. 2a is very similar to that of the pristine graphene. The phonon DOS is mostly related to the number of carbon atoms in the unit cell. Since the fill factor of the antidot lattice is ~80%, no drastic changes are observed in the phonon DOS calculation. The transmission of the antidot lattice, on the other hand, is drastically reduced from the pristine graphene value as shown in Fig. 2b. Introduction of antidots changes the phonon group velocity and results in phonon reflections or possible localization behavior near the antidot edges, which reduces the transmission considerably. This signals a drastic change in the thermal conductance as well, as we will show later on. The important result from this observation, however, is that even small antidots, compared to the filled area of the graphene can have a large effect on the thermal properties, something which could be proven useful for the design of efficient thermoelectric devices for which low thermal conductivity is needed.

The reduction in the thermal conductance has also some dependence on the exact geometry of the antidots. The antidot shape, the number of edge atoms, the distance between neighboring antidots and the type of the edges (zigzag or armchair) have some effect on the transmission probabilities. To investigate the effect of these parameters, we compare the thermal conductance of a hexagonal, a rectangular, and a triangular GAL with similar fill-factors of 81%, 80%, and 84%, respectively. The phonon DOS and transmission probabilities are shown in Fig. 3a and 3b respectively. The three different structures are labeled Hex(8,96,24) – solid/blue, Rect(8,104,28) – dashed/red, and IsoTri(8,90,30) – dashed-dot/green, respectively. The DOS in all three GALs in Fig. 3a is of similar magnitude as expected since the fill factor is nearly the same. The transmission probabilities, on the other hand, indicate some variations depending on the shape of the GALs as shown in Fig. 3b. The Hex(8,96,24) has the highest and IsoTri(8,90,30) the lowest transmission probabilities through most of the phonon energy spectrum.

The difference in the transmission, however is not large. To compare the differences in the transmission of the three different GALs, in Fig. 4 we plot the transmission probabilities of the three GALs normalized to the transmission of the hexagonal GAL, which has the highest transmission. From this figure, it is clear that the transmission of the rectangular GAL is ~10-20% lower than that of the hexagonal one in most of the energy spectrum. The transmission of the triangular GAL is ~40% lower.

There are two possible reasons why the transmission of the IsoTri(8,90,30) GAL is smaller compared to the Hex(8,96,24) GAL. The first one is geometrical in nature. The triangular GAL has a larger circumference. The triangular GAL has 30 edge atoms for each antidot, whereas the hexagonal one has 24 edge atoms. In addition, the distance between the nearest neighbor antidots in the triangular antidot case is smaller. This could be the reason behind the lowest transmission probability for the triangular antidot lattice. The second reason is related to the type of the edges that form the antidot. In a recent work, Tan et al. theoretically showed that the phonon dispersion in zigzag edge graphene nanoribbons is more dispersive compared to the phonon dispersion in armchair ribbons [30]. Phonons, therefore, tend to localize more around armchair edges. Viewing each edge in the GALs as the edge of a short ribbon, one can explain the differences between the thermal conductances. The phonon dispersion of Hex(8,96,24),

Table 1: Comparison of the thermal conductances of different GALs. The results are normalized to the thermal conductance of pristine graphene.

Structure	Normalized thermal conductance
Pristine Graphene	1
Hex(8, 96, 24)	0.2202
IsoTri(8, 90, 30)	0.1464
Rect(8, 104, 28)	0.1894

which has only zigzag boundaries is more dispersive, whereas that of the IsoTri(8,90,30) antidot which has only armchair edges is less dispersive. The transmission probability is, therefore, larger in Hex(8,96,24). The Rect(8,104,28) has both zigzag and armchair edges. Its circumference, with 28 atoms is larger than that of the hexagonal antidot but smaller than that of the triangular one. Therefore, its phonon transmission probability lies between those of the Hex(8,96,24) and IsoTri(8,90,30) structures. Although further work is needed in order to clearly identify the reasons behind these variations in the transmission, our results indicate that the geometry and the edge types would play a part in this.

The reduction in the transmission probabilities of the antidot lattices compared to pristine graphene, as well as the differences in the transmission between the different antidot shapes will result in different thermal conductances as well. The thermal conductance is calculated using the Landauer formalism in the ballistic limit as shown in Eq. 3. Table 1 summarizes the results for the thermal conductance of GALs normalized to the pristine graphene conductance. The thermal conductance of the GALs is reduced to ~20% of the original pristine graphene value, which indicates that such channel could be utilized for thermoelectric applications, where such large reductions in the thermal conductance are highly desirable.

4. CONCLUSION

The phonon density-of-states, transmission probability and ballistic thermal conductance for hydrogen-passivated graphene antidot lattices of ~80% fill factor was theoretically investigated. First principle calculations were used for the phonon bandstructure, and the ballistic Landauer approach for phonon transport calculation. We show that the ballistic thermal conductance can decrease up to ~5X by introducing antidots in the pristine graphene lattice. Geometrical parameters, such as area, circumference, and boundary edge of antidots could also be utilized as design parameters for achieving additional thermal conductance reduction optimization, although small. Among all the GALs studies in this work, the triangular antidot has the lowest thermal conductance, possibly because of its longest boundary and its smallest distance between neighboring antidots at the same fill factor compared to hexagonal or rectangular geometries.

5. ACKNOWLEDGEMENTS

This work was supported by the Austrian Climate and Energy Fund (Contract No. 825467) and the Austrian Science Fund FWF (Contract F2509).

6. REFERENCES

[1] G. Nolas, J. Sharp, H. Goldsmid, *Thermoelectrics: Basic Principles and New Materials Developments*, Springer, 2001.
[2] H. Goldsmid, *Introduction to Thermoelectricity*, Springer, 2010.
[3] L. Weber, E. Gmelin, *Appl. Phys. A* **53**, 136 (1991).
[4] A.I. Hochbaum, R. Chen, R. Delgado, W. Liang, E. Garnett, M. Najarian, A. Majumdar, P. Yang, *Nature* **451**, 163 (2008).
[5] A. Boukai, Y. Bunimovich, J. Tahir-Kheli, J.K. Yu, W. Goddard, J. Heath, *Nature* **451**, 168 (2008).
[6] R. Venkatasubramanian, E. Siivola, T. Colpitts, B. O'Quinn, *Nature* **413**, 597 (2001).
[7] T.C. Harman, P.J. Taylor, M.P. Walsh, B.E. LaForge, *Science* **297**, 2229 (2002).
[8] Z. Xiaofang, J. Zuimin, L. Jianhui, T. Xiaodong, C. Qingming, Z. Hui, Z. Pengxiang, *J. Phys. D: Appl. Phys.* **42**, 225303 (2009).
[9] K. Novoselov, A. Geim, S. Morozov, D. Jiang, Y. Zhang, S. Dubonos, I. Grigorieva, *Science* **306**, 666 (2004).
[10] L. Falkovsky, *IOP J. Phys.:Conf. Ser.* **129**, 012004 (2008).
[11] A. Balandin, S. Ghosh, W. Bao, I. Calizo, D. Teweldebrhan, F. Miao, C. Lau, *Nano Lett.* **8**, 902 (2008).
[12] K. Kim, Y. Zhao, H. Jang, S. Lee, J. Kim, K. Kim, J.H. Ahn, P. Kim, J.Y. Choi, B. Hong, *Nature* **457**, 706 (2009).
[13] J.H. Chen, C. Jang, S. Xiao, M. Ishighami, M. Fuhrer, *Nature Nanotech.* **3**, 206 (2008).
[14] J.H. Seol, I. Jo, A.L. Moore, L. Lindsay, Z.H. Aitkenhary, M.T. Pettes, X. Li, Z. Yao, R. Huang, D. Broido, N. Mingo, R.S. Ruoff, L. Shi, *Science* **328,** 213 (2010).
[15] M. Han, B. Ozyilmaz, Y. Zhang, P. Kim, *Phys. Rev. Lett.* **98**, 206805 (2007).
[16] T.G. Pedersen, C. Flindt, J. Pedersen, A.P. Jauho, N.A. Mortensen, K. Pedersen, *Phys. Rev. B* **77**, 245431 (2008).
[17] A.A. Balandin, S. Ghosh, W. Bao, I. Calizo, D. Teweldebrhan, F. Miao, C.N. Lau, *Nano Lett.* **8**, 902 (2008).
[18] J. Hone, M. Whitney, C. Piskoti, A. Zettl, *Phys. Rev. B* **59**, R2514 (1999).
[19] H. Sevincli, G. Cuniberti, *Phys. Rev. B* **81**, 113401 (2010).
[20] Z. Guo, D. Zhang, X.G. Gong, *Appl. Phys. Lett.* **95**, 163103 (2009).
[21] Y. Ouyang, J. Guo, *Appl. Phys. Lett.* **94**, 263107 (2009).
[22] H. Zhang, G. Lee, A.F. Fonseca, T.L. Borders, K. Cho, *Journal of Nanomaterials* **2010**, 537657 (2010).
[23] J. Bai, X. Zhong, S. Jiang, Y. Huang, X. Duan, *Nature Nanotech.* **5**, 190 (2010).
[24] J. Eroms, D. Weiss, *New J. Phys.* **11,** 093021 (2009).
[25] D.W. Boukhvalov, M.I. Katsnelson, A.I. Lichtenstein, *Phys. Rev. B* **77**, 035427 (2008).
[26] D. Sanchez-Portal, P. Ordejon, E. Artacho, J.M. Soler, *Int. J. Quantum Chem.* **65**,453 (1997).
[27] J.P. Perdew, K. Burke, M. Ernzerhof, *Phys. Rev. Lett.* **77**, 3865 (1996).
[28] S. Datta, Quantum *Transport: Atom to Transistor*, Cambridge University Press, Cambridge, 2005.
[29] Y. Ouyang and J. Guo, *Appl. Phys. Lett.* **94**, 263107 (2009).
[30] Z. Tan, J. Wang, and C. Gan, *Nano Lett.* **11**, 214 (2011).